IJITCE

ISSN 2347- 3657

International Journal of Information Technology & Computer Engineering

Email : ijitce.editor@gmail.com or editor@ijitce.com

International Journal of Information Technology & Computer Engineering

ISSN 2347–3657
Volume 12,Issue 2,May 2024

DESIGN OF A CPW FED POLYGONAL SUPER WIDEBAND ANTENNA WITH DEFECTED ASYMMETRICAL GROUND STRUCTURE

Project Guide
Dr.A.RaghavaRaju
Associate Professor
Battula Aneesha

Burri Esther Rani

Akaramsetty Vijaya Naga Durga

Tonduru Swapna

ABSTRACT This research introduces a super-wideband antenna for wireless sensor networks that is fed by a coplanar waveguide. The investigated low-profile design has been prototyped on a single-sided FR4 microwave substrate and consists of two asymmetrical ground planes and a modified bow-tie-shaped vertical patch. At 3.035 GHz, the lowest frequency in the operational band, the expected antenna measures 0.25λ × 0.20λ in overall dimensions. A 140.56% operational band from 3.035 to 17.39 GHz was achieved by the investigated antenna, which was made possible by the vertical radiator's good coupling with the two coplanar ground planes. With an average gain of 4.56 dBi and an average efficiency of 76.62%, the antenna that is being described exhibits radiation patterns that are almost omnidirectional across its entire operational range. The antenna has a flat group delay, little phase distortion, a good responsiveness of the transfer function, and a high fidelity factor. Because of all these features, the investigated antenna is a strong candidate for use in wireless sensor node applications.

INDEX TERMS Antenna, bow-tie shaped radiator, coplanar ground plane, CPW-fed, sensor networks, sensor node.

INTRODUCTION

I. One of the most exciting and quickly developing wireless technologies is the wireless sensor network (WSN), which consists of a collection of nodes distributed throughout space. Environmental sensing, healthcare monitoring, area monitoring, air pollution, water quality, industrial monitoring, landslide, forest fire, battlefield, and intruder detection are some of the possible uses of WSNs [1-3].

DEPARTMENT OF ELECTRONICS AND COMMUNICATION ENGINEERING

Guntur Engineering College

Jawaharlal Nehru Technological University, Kakinada.

ISSN 2347–3657
Volume 12,Issue 2,May 2024

II. The sensor network's nodes take readings from their environments, analyze them, and then wirelessly send their findings to one another and the base station. All of the nodes in a WSN rely on a single source of energy, the battery, to keep them running. When it comes to transceiver power consumption, the node antenna is a key component. A powerful power supply is required for signal transceiving across long distances. The design of a suitable node antenna that establishes an efficient low powered communication system in sensor network is a challenging task. As the antenna in the node occupies the most area of the whole node and it is, therefore, necessary to miniature the antenna to lessen the overall node size without compromising its performances. Moreover, to transceive the data in all directions, the radiation patterns of the node antenna should be omnidirectional.

In recent years, the super-wideband (SWB) and ultra- wideband (UWB) antennas have attracted more attention due to their numerous advantages including very wide operating band, low-profile, light-weight, inexpensive, high data transmission rate, ease of integration with MICs or MMICs. Hence, these antennas are the most favorite choice to be used as node antenna in wireless sensor network applications. However, the design of an appropriate SWB/UWB node antenna is still a difficult task. A suitable SWB/UWB node antenna must be small, planar, inexpensive, and should work over a wide range of frequencies with omnidirectional radiation characteristics. At the same time, they should exhibit good time-domain characteristics to minimize signal distortions.

Recently good numbers of SWB/UWB patch antennas have been reported [4 - 23]. Different methods such as the use of the thick substrate and substrate with low permittivity, incorporation of slit/slot in the radiator/ground plane, and optimization-based procedures have been reported to design and enlarge the bandwidth of microstrip patch antennas [24 -25]. Microstrip line feeding [5, 7, 8, 10-14, 16, 18, 20, 23]
and coplanar waveguide (CPW) [4, 6, 9, 15, 17, 19, 21 - 22] feeding techniques are also employed to achieve super/ultra/wide operating band. For example, in [5], a symmetric open slot antenna was designed for UWB application. Using the U-shaped feedline, the reported design attained a working band ranging from 3.1-13.2 GHz. The antenna reported in [5] demonstrates better miniaturization with an overall footprint of 580 mm^2 when compared to the patch antenna with modified partial ground plane [7], a diamond-shaped radiating patch with partial multi-slotted ground plane [8], bird face-shaped patch with a single slotted limited ground plane[10], modified slotted U-shaped antenna [11], hibiscus petal-shaped radiator and small trapezoid ground plane [12], modified annular ring-shaped

ISSN 2347–3657
Volume 12,Issue 2,May 2024

radiator with rectangular semi ground [13], corner truncated rectangular patch with single slotted ground plane [14], the circular patch with iterations of a hexagonal slot [16], annular ring-shaped radiator with small ground plane [18], circular radiator with hexagonal-square-shaped fractal geometry and partial ground plane [20], and semi-circular radiator with small trapezoid ground plane [23]. However, in microstrip line-fed antennas, the space available on both sides of the substrate is not entirely used resulting in elevated fabrication cost during mass production.

In contrary to microstrip line-feeding, CPW-fed antennas utilize most of the space around the patch [17]. In the CPW-fed antenna, the patch and the ground plane are printed on the same side of the substrate. CPW technique is mainly useful for fabricating antenna, due to the presence of the center radiator and the proximity of the ground planes. CPW-fed antennas demonstrate higher operating bandwidth, less dispersion, and lower radiation leakage than microstrip line-fed antennas. Moreover, it is easy to prototype the CPW-fed antenna as etching is done on one side of the microwave substrate and it does not require any via holes. In [4], a CPW-fed UWB monopole antenna was reported. Using two L-shaped coplanar open ground stubs, the antenna attained a working band of 3.1-13.2 GHz. A CPW-fed antenna with the polygon-shaped radiator was presented in [6]. To enhance the bandwidth, in this design small fractal elements have been added to the patch that helps it to achieve a bandwidth of 7.85 GHz. In [9], fractal geometry was adopted in the patch to achieve an ultra-wide operating band of 2.5 - 10 GHz. A CPW- fed umbrella-shaped antenna was reported in [15]. Having a total area of 30 × 35 mm^2, the designed antenna achieved a relative bandwidth of 123%. In [17], a wideband antenna on a defected crown-shaped FR4 substrate was designed. Using an extended U-shaped patch and two coplanar ground planes this antenna attained an operating band of 4.5-13.5 GHz. A CPW-fed UWB monopole antenna with a triangular-shaped radiator was presented in [19]. To enhance the working band, a top-cross-loop is used to connect the two coplanar ground planes. However, it possesses an overall size of 1650 mm^2. In [21], a spiral antenna with coplanar strips was reported. But its larger size makes it difficult to integrate within the sensor node. A CPW fed patch antenna that comprised of the semi-circular patch with slots and two rectangular coplanar ground planes was presented in [22]. However, it possesses a dimension of 40 × 53.3 mm^2 and not suitable for sensor applications. Though most of the above-mentioned antennas successfully achieved a super/ultra/wide operating band, some of them possess a large footprint and not suitable for wireless sensor nodes.

ISSN 2347–3657
Volume 12,Issue 2,May 2024

A small SWB antenna for wireless sensor nodes is presented and prototyped in this paper. The compactness of the proposed low-profile antenna is achieved by the effective coupling of two asymmetrical coplanar ground planes and a CPW-fed modified bow-tie-shaped vertical patch. With a total footprint of 490 mm^2, the studied antenna is much smaller than many reported antennas and achieved good gain, efficiency, and demonstrations almost omnidirectional radiation patterns over the entire working band of 3.035-17.35 GHz. The proposed antenna features with advantages of low fabrication cost, small, easy prototyping, and easy integration with RF circuitry is suitable for wireless sensor network applications.

III. ANTENNA DESIGN

The foot-print of the anticipated antenna is displayed in Fig. 1. The antenna is designed only on the top side of the FR4 microwave substrate with dielectric constant 4.6, thickness 1.6 mm, and loss tangent 0.02. The metallization used for the proposed antenna is 0.035 mm copper cladding which is commercially available in the FR4 substrate and there is no copper on the backside of the substrate which provides an advantage for portable communication devices due to low manufacturing cost. The antenna is comprised of a vertical bow-tie-shaped patch with unequal wings and is fed by a CPW strip line of width w_1. On both sides of the feed line, a gap g is kept between the feed line and the coplanar ground plane. The width of the feed line and gap are so chosen that the characteristics impedance of the presented antenna becomes equal to 50 ohms for the used microwave substrate. The width and length of the tapered transitional wing of the bow-tie-shaped radiator are respectively w_2 and l_2 while the width and length of the upper

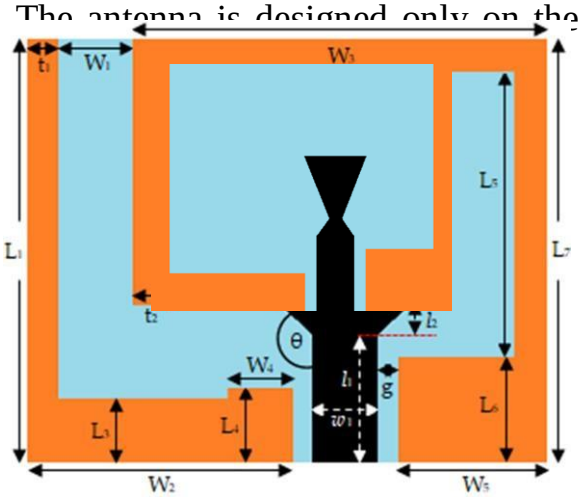

Figure 1. Design layout of the proposed antenna.

its lower end is connected to the CPW feed line of length l_1. Instead of using the complex

ISSN 2347–3657
Volume 12,Issue 2,May 2024

matching network to attain a very wide operating band, the presented asymmetric antenna is fed by an SMA connector which acts as a self- resonator with a very compact dimension [26].

In the studied design, two partial coplanar ground planes are used which not only act as an elementary source of radiation but also improves the impedance matching. An L- shaped ground plane is placed at the left side of the bow- tie-shaped patch that is comprised of one vertical arm of size $(L_1 - L_3) \times t_1$ and one horizontal arm having two parts of dimensions $(W_2 - W_4) \times L_3$ and $W_4 \times L_4$. On the right side of the patch, a modified inverted U-shaped ground plane is positioned that consists of four parts of dimensions $t_2 \times L_2$, $W_3 \times t_2$, $t_2 \times L_5$, and $W_5 \times L_6$. The determined optimal parameters of the anticipated antenna having a compact volumetric size of $24.5 \times 20 \times 1.6$ mm^3 are listed in Table I.

TABLE I
PARAMETERS OF THE PROPOSED ANTENNA

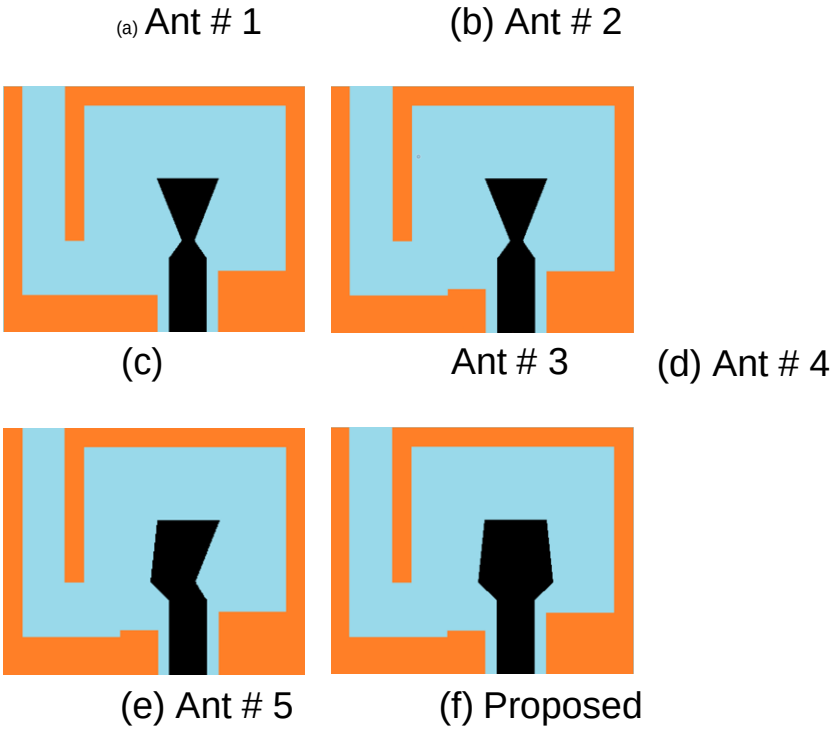

Figure 2. Evolution steps of the studied antenna.

bow-tie-shaped patch, one L-shaped coplanar ground plane, and one inverted L-shaped coplanar ground plane placed on the left and right sides of the patch respectively. A rectangular strip line of dimension $W_3 \times t_2$ is horizontally added to the top edge of the vertical arm of the inverted U- shaped coplanar ground plane to form the Ant # 2 as shown in Fig. 2(b). As in Fig. 2(c), Ant # 3 is formed by vertically adding another strip line of size $t_2 \times L_2$ to the last end of the inverted U-shaped ground plane of Ant # 2. A small rectangle of dimension $W_4 \times$

ISSN 2347–3657
Volume 12,Issue 2,May 2024

(L_4 -L_3) is added to the last end of the L-shaped coplanar ground plane to form Ant # 4 as shown in Fig. 2(d). To form Ant-5, a triangular portion is added to the left lower end of the bow-tie-shaped radiator. Finally, another triangular portion is added to the right lower end of the bow-tie-shaped radiator to form the proposed antenna of Fig. 2(f).

A. *ANTENNA EVOLUTION*

To comprehend the working mechanism, six evolution stages of the studied antenna are depicted in Fig. 2 and the corresponding S-parameter and input impedance of these stages are respectively presented in Fig. 3. In Fig. 2(a) Ant # 1 is depicted which is consists of a CPW-fed vertical

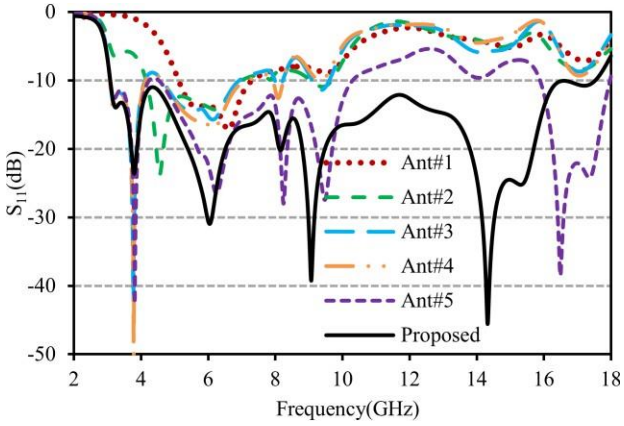

Figure 3. Simulated S11 for different evolution steps.

achieved a -10dB operating band of 5.12 - 7.30 GHz where the input impedance is very much close to 50 Ω characteristics impedance line. The addition of horizontal strip-line to the inverted L-shaped ground plane of Ant # 1 (i. e. Ant # 2 excited an additional resonance at around 9.17 GHz and the first resonance moved to the lower band resulting in the exhibition of dual operating bands of 4.15 -
6.99 GHz and 9.05 - 9.68 GHz. The impedances in these bands are also better than that of Ant # 1. When the vertical strip-line is added to the inverted L-shaped coplanar ground plane of Ant # 2 (Ant # 3), Fig. 3 shows that inclusion of vertical strip-line excites two additional resonances at around 3.74 GHz and 8 GHz and the Ant # 3 achieves four working bands of 3.08 - 4.12 GHz, 4.63 - 6.92 GHz, 7.99 - 8.22 GHz, and 9.10 - 9.61 GHz covering WiFi, WiMAX, WLAN, UWB, LTE, and 5G sub-6 GHz bands. When a triangular portion is added to the lower end of the radiator (Ant # 5), two additional resonant modes are excited at around

ISSN 2347–3657
Volume 12,Issue 2,May 2024

16.48 GHz and 17.22 GHz as depicted in Fig. 3. Moreover, the second, third, and fourth resonances exhibit better performances in-terms of S_{11} due to proper impedance matching. When another triangular portion is added to the right lower end of the radiator of Ant # 5 (the proposed antenna), a significant improvement of impedance matching over the 3 - 18 GHz band has been observed. As in Fig. 3, seven distinct resonant modes have been observed at around 3.25 GHz, 3.80 GHz, 6.0 GHz, 8.19 GHz, 8.99 GHz, 14.31 GHz, 16.75 GHz and merging of these near-by resonances resulting in the achieving of the super-wide working band of 3.09 - 17.54 GHz which makes it suitable for WiMAX, WLAN, UWB, C-, X-, and Ku-band applications.

B. SURFACE CURRENT DISTRIBUTIONS

To realize the operating principle, the surface current distributions at resonant frequencies of 3.25, 6.0, 8.19, 8.99, 14.31, and 16.75 GHz are shown in Fig. 4. In the figure, the arrow signs indicate the direction of the current path while the intensity of the current is represented by the colour scale. In the scale, the blue color region represents the current null and the red color indicates the strongest current. As shown in the first one of Fig. 4, at 3.25 GHz, the current is stronger in vertical (*Y*-direction) and horizontal (*X*-direction) arms of L-shaped ground and upper horizontal arm of the inverted U-shaped ground plane. As shown in the second one of Fig. 4, at 6.0 GHz stronger current flows in the lower horizontal arms and two outer vertical arms of the two ground planes, and the directions of current in corresponding arms in two ground planes are

opposite to each other. Moreover, stronger flows of current have also been observed in the CPW-fed patch and feedline. As the frequency increases the current concentration in horizontal directions of the antenna gradually decreases. This low concentration of current develops a high cross-polarized component especially in the *H*-plane pattern which has been reported in [26]. Furthermore, the concentration of current in the modified bow-tie-shaped radiator and the CPW-feedline are increasing with the frequency which plays a vital role in the flow of vertical (*Y*-direction) current. Because of these higher vertical currents, the co-polarized component significantly enhances the radiated field patterns. From the current distributions, it is observed that at low frequencies the currents are stronger in the vertical arms of the coplanar ground planes while at higher frequencies strongest currents have been observed at lower horizontal arms of the ground planes and bow-tie-shaped radiator. As conclusions, using a modified bow-tie-shaped radiator and two asymmetric ground planes, the studied antenna achieved the desired super-wide operating band.

ISSN 2347–3657
Volume 12,Issue 2,May 2024

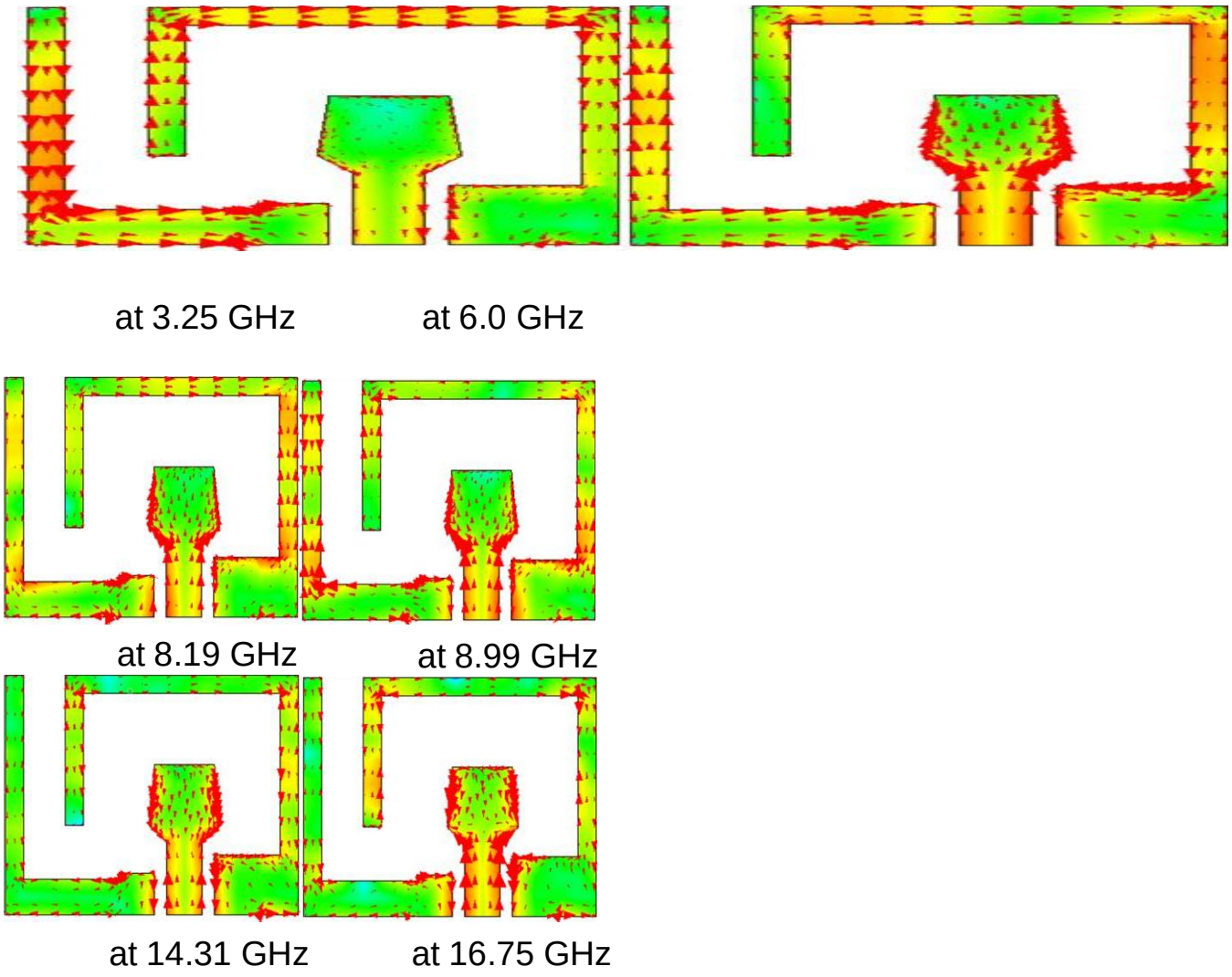

Figure 4. Surface current distribution at 3.25 GHz, 6.0 GHz, 8.19 GHz, 8.99 GHz, 14.31 GHz and 16.75 GHz.

c. *PARAMETRIC STUDIES*

To reveal the behavior of the proposed antenna, the effects of L_1, L_2, L_7, W_3, l_1, and l_3 are analyzed using IE3D software and presented in Fig. 5. The simulated S_{11} with different values of L_1, the length of the vertical arm of the L-shaped coplanar ground plane is shown in Fig. 5(a). When the value of L_1 increases, the lower cutoff frequency shifts to some lower value due to the increased current path. Moreover, as the value of L_1 moves away from the optimized one, dual notch bands are generated at the two edge frequencies of the operating band resulting in the decrement of overall bandwidth. Trading off the bandwidth and the matching, L_1 = 20 mm is taken as the optimized value. Fig. 5(b) depicted the S_{11} responses for different values of L_2, the length left vertical arm of the inverted U- shaped

ISSN 2347–3657
Volume 12,Issue 2,May 2024

ground plane. As the value of L_2 increases or decreases from the optimized value of 11 mm, the antenna performances become poorer in-terms of S_{11}. The S_{11} responses with different values of L_7, the length of the right vertical arm of the inverted U-shaped ground plane are shown in Fig. 5(c). It is seen in the plot that a lower value of L_7 gives a narrower operating band whereas a value higher than the final value (20 mm) exhibits poor matching at around 7.41 GHz. The higher cutoff frequency also shifted to the lower band as the value of L_7 becomes smaller or larger than 20 mm. Fig. 5(d) depicts the simulated S_{11} forvarious values of W_3, the length of the upper horizontal arm of the inverted U-shaped coplanar ground plane. It can be seen that for values of W_3 lower and higher than the

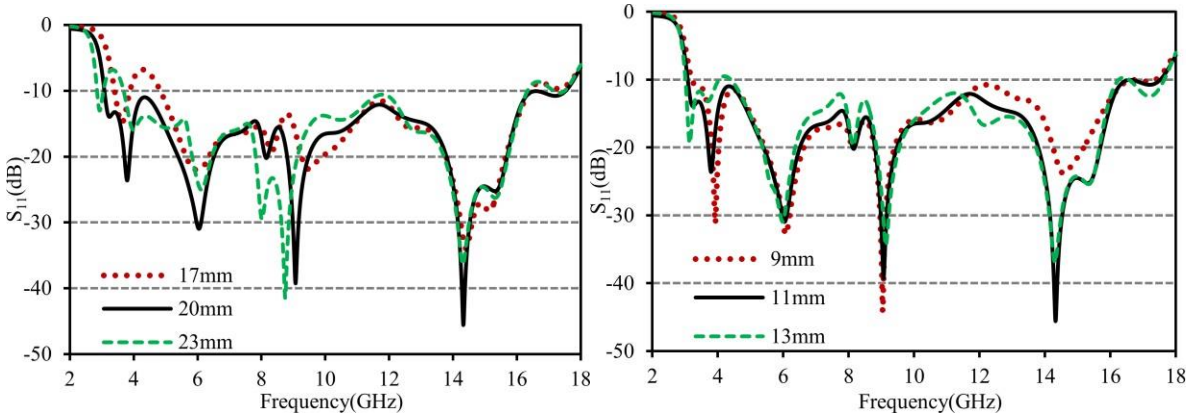

(a)

(b)

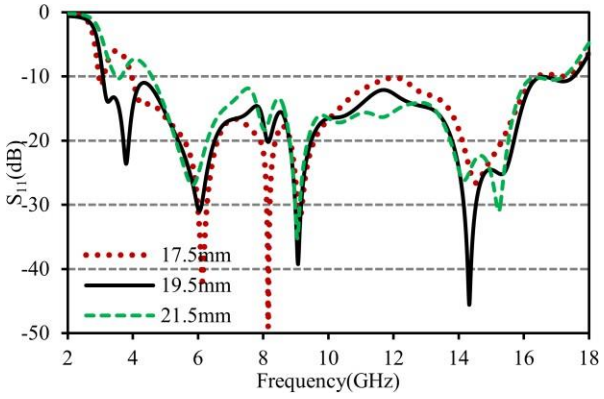

ISSN 2347–3657
Volume 12,Issue 2,May 2024

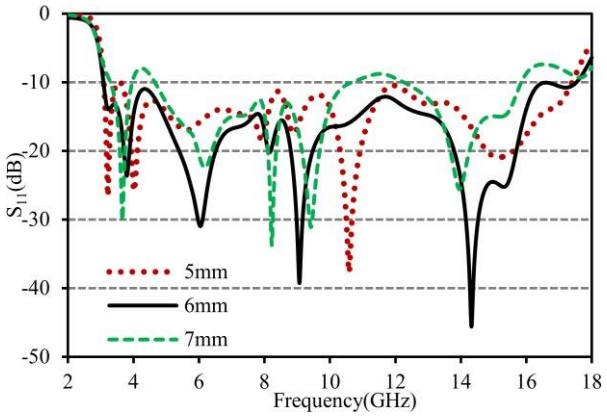

(e)

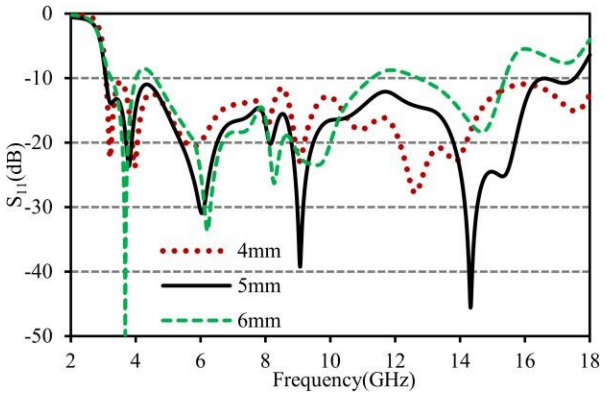

matching in between 3 to 4 GHz become worse resulting in the narrowing of the operating band. Moreover, the increment of W_3 moves the lower cutoff frequency towards the higher band. In this design, the value of W_3 is taken as 19.5 mm to prototype the anticipated antenna. The effects of l_1 (length of CPW strip- line) and l_3 (length of the vertical radiator) are respectively plotted in Fig. 5(e) and 5(f). From figures, it is seen that if the values of l_1 and l_3 increase from the optimized ones (6 mm and 5 mm respectively), poor impedance matching have been observed at around 4 GHz, 11/12 GHz and 16 GHz results in the exhibition of three distinct operating bands. Moreover, the higher cutoff frequency significantly sifted towards the lower band as the values of l_1 and l_3 increases from their final values. From the above parametric studies, it can be noted that the coplanar ground planes play an important role in lower cutoff frequency while the CPW-fed modified bow-tie-shaped radiator controls the higher cutoff frequency of the proposed antenna which has demonstrated in Fig. 4.

IV. RESULTS AND DISCUSSION

A. *FREQUENCY- DOMAIN CHARACTERISTICS*

The design of the antenna presented in the paper has been prototyped for the substantiation of the results obtained from IE3D and CST MWS software with

ISSN 2347–3657
Volume 12,Issue 2,May 2024

optimal parameters and is shown in the inset of Fig. 6. The input impedance characteristic of the antenna is measured using N5227A PNA microwave network analyzer in the frequency spectrum of 10 MHz - 67 GHz. The comparison between the simulated and measured S_{11} is presented in Fig.
6. Good agreements have been observed between the simulated and measured results. It is evident from the plot that, the measured results offer an operating bandwidth of
14.36 GHz from 3.035 GHz to 17.39 GHz which is equivalent to a fractional bandwidth of 140.56%. The differences between the two simulated results are mainly due to the unequal mesh sizes. The discrepancies between the simulated and measured results might be arises due to

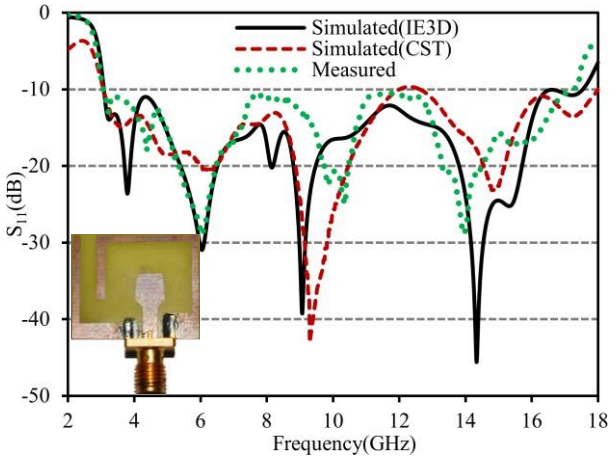

Figure 6.
Simulated and measured S11 of the studied antenna.

the prototyping and measurement inaccuracies. Moreover, in simulation, the antenna is fed by a lumped port which is assumed to be loss-free and of 50 Ω characteristics impedance for the entire frequency spectrum of 2 - 18 GHz which is very tough to achieve during the prototyping, especially on low-cost FR4 substrate. The radiation characteristics of the studied super-wideband antenna are measured in an anechoic chamber using near field antenna measurement system StarLab from MVG. The peak gain in the bore-sight (+*Z*) direction is illustrated in Fig. 7(a). As predicted, the peak gain increases with frequencies. A good matching has been seen between the simulated and measured values. The antenna achieved a maximum gain of
6 dBi at 16.80 GHz and an average of 4.56 dBi. As the antenna is suitable for wireless sensor nodes, the achieved gain is within the acceptable limit. The gain of the presented antenna can be enhanced using expansive Rogers/Duroid substrate with low loss tangent. The simulated and measured radiation efficiency is displayed in Fig.

ISSN 2347–3657
Volume 12,Issue 2,May 2024

7(b). It is clear to see that the average radiation efficiency of the studied antenna is 76.62% and the maximum efficiency is 89.36%. In the efficiency curve, a null has been observed which maybe due to the limitations of measurement.

Moreover, at the null frequency, the SMA connector has a degenerative effect on the small antennas which has been reported in many CPW-fed antennas [27 - 28].

The measured 2D normalized *E*-and *H*-field radiation patterns of the studied antenna at 3.25 GHz, 6.0 GHz, 8.19 GHz, 8.99 GHz, 14.31 GHz, and 16.75 GHz are

respectively depicted in Fig. 8 and Fig. 9. In the figures, the solid black line represents the co-polarized component, E_θ while the dashed red line represents the co-polarized component, E_φ. It is clear to see in the figures that the anticipated antenna exhibit slightly deviated omnidirectional radiation patterns. Despite the asymmetrical shape, the radiation patterns of the studied antenna over the entire operating band are almost symmetrical with some nulls. In comparison to the other asymmetric CPW-fed antennas [27 - 30], the studied antenna demonstrates stable and ripple-free radiation patterns even at higher frequencies of 14.31 GHz and 16.75 GHz which is mainly due to the concentration of maximum currents along with the vertical bow-tie-shaped patch. In the *E*-plane pattern as shown in Fig. 8, the cross-polarized (E_φ) component is remarkably small and the main beams are

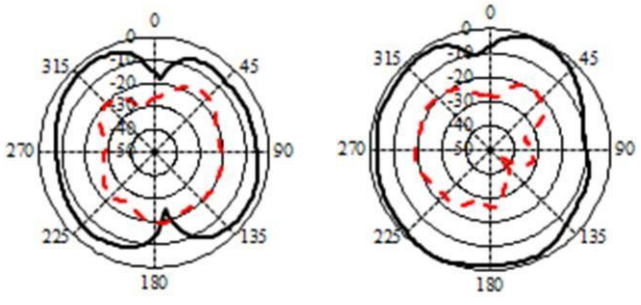

at 3.25 GHz

at 6.0 GHz

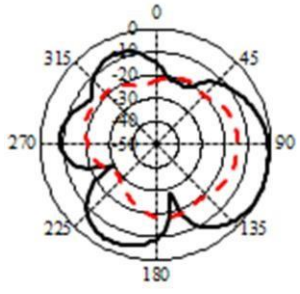

at 8.19 GHz

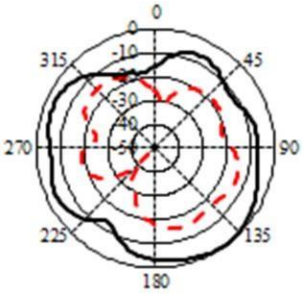

at 8.99 GHz

ISSN 2347–3657
Volume 12,Issue 2,May 2024

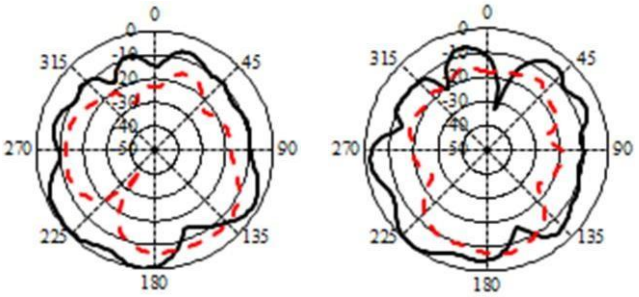

at 14.31 GHz at 16.75 GHz

Figure 8. Measured *E*-plane patterns at different frequencies.

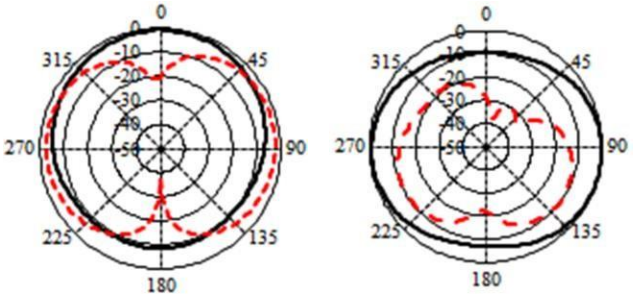

at 3.25 GHz at 6.0 GHz

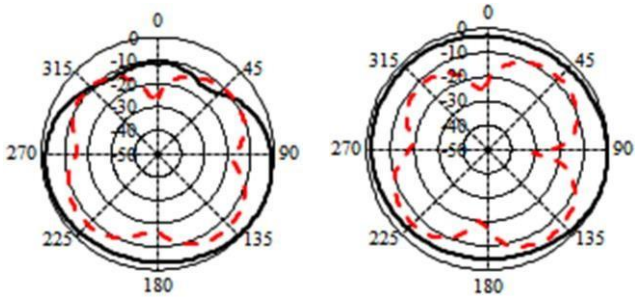

at 8.19 GHz at 8.99 GHz

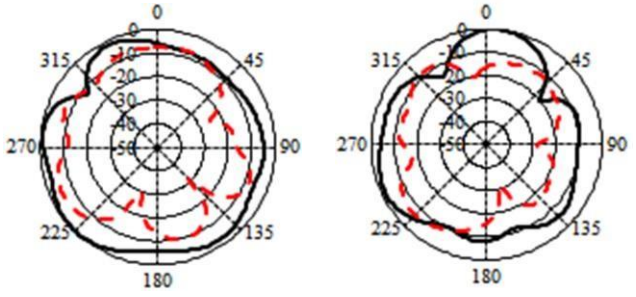

at 14.31 GHz at 16.75 GHz

Figure 9. Measured *H*-plane patterns at different frequencies.

ISSN 2347–3657
Volume 12,Issue 2,May 2024

positioned towards the *Z*-direction (90^0, 270^0) which makes the proposed antenna suitable for the handheld sensor network devices as it can help to avoid the interferences with other EM radiations. In the *H*-plane pattern as shown in Fig. 9, the cross-polarization component is higher, especially at lower frequencies. This is maybe due to the strong horizontal components of the surface currents. The contribution to the antenna radiation is mainly from vertical components (in *Y*-direction) of the surface currents. Instead of contributing to the co-polarized radiation in the *H*-plane pattern, the currents along the horizontal arms of the L- shaped and inverted U-shaped ground planes enhance the cross-polarized component [26]. However, at higher frequencies, the cross-polarization component decreases as the currents in horizontal arms of the coplanar ground planes decreases and the size of the antenna becomes larger in comparison to the wavelength.

B. TIME-DOMAIN CHARACTERISTICS

Since SWB as well as UWB systems, directly transmit narrow pulses rather than continuous wave, the time

domain characteristic of the SWB/UWB antenna is very vital. In contrast to the narrow-band counterpart, good time-domain behavior is a basic requisite of SWB/UWB antennas. The antenna features can be optimized to avoid the undesired distortions. In the time domain analysis, the transmitting and receiving antennas are placed at a distance of 240 mm apart in face to face and side by side orientations.

The transmitting antenna is excited by a Gaussian pulse and the transmitted impulse is received by the second antenna. The normalized transmitted and received signals in both orientations are displayed in Fig. 10 (a). Using the normalized transmitted and received pulses, the fidelity factor (FF) that defines the correlation between the transmitted and received pulses can be calculated using [31
- 32]

ISSN 2347–3657
Volume 12,Issue 2,May 2024

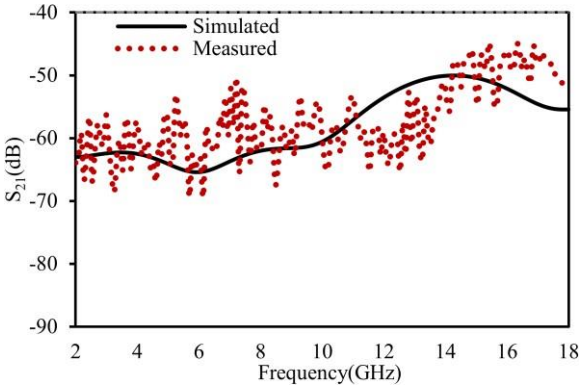

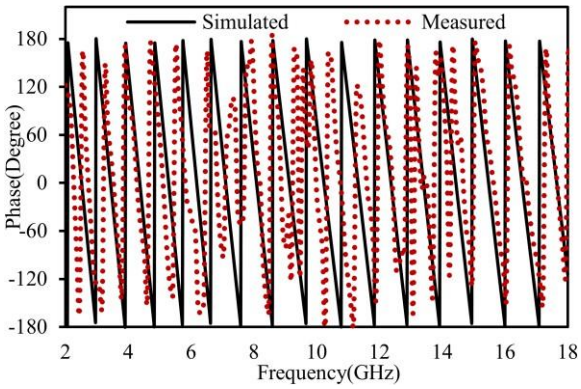

where $S_T(t)$ and $S_R(t)$ are respectively the transmitted and received pulses and τ is the group delay. The calculated fidelity factor in the face to face and side by side orientations are respectively 94.3% and 96.6% which confirm that in side by side orientation the correlation is more than that in the face to face orientation. This finding suggests that in side by side orientation the studied antenna

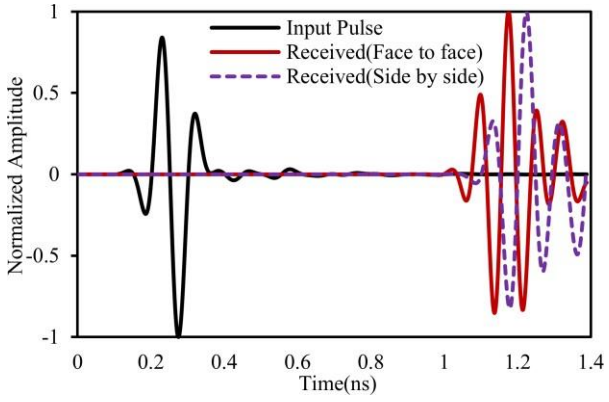

(a)

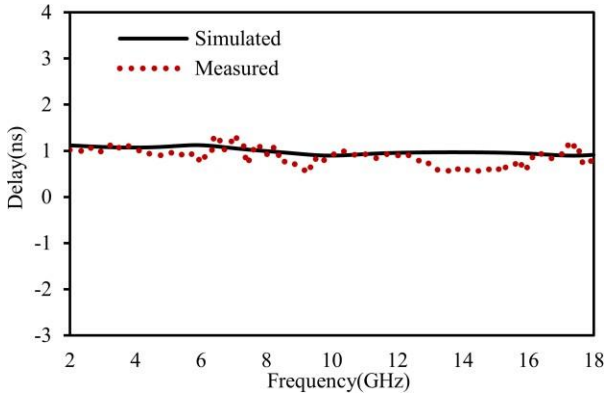

(b)

ISSN 2347–3657
Volume 12,Issue 2,May 2024

(d)

Figure 10. (a) Normalized transmitted and received pulses, (b) Group delay, (c) Transfer function (S21), and (d) Phase of S21.

transmits the exciting pulse with less distortion in comparison to the other orientation. The group delay is defined as the negative derivative of the phase response with respect to frequency. It indicates the time delay of an impulse signal at different frequencies. The simulated and measured group delay of the anticipated antenna in face-to- face orientation is shown in Fig. 10(b) which indicates that over the entire operating band the measured group delay varies between 0.52 ns and 1.35 ns with an average of 0.87 ns. These limits of group delay ensure the phase linearity over the operating band which is a vital requisite of sensor network applications [33]. The simulated and measured amplitude of transfer function, S_{21} is shown in Fig. 10(c). The ripples in the measured result are mostly attributed to the noise in the measurement which can be minimized by implementing the averaging algorithm. It is clear to see in Fig. 10 (c) that the value of S_{21} is better than -45 dB over the entire working band. This higher value of S_{21} suggests that the transfer of signal between two identical radiators is not correlated [34]. Fig. 10(d) depicts the simulated and measured phase variation of S_{21}. It is seen that the phase is almost linear across the operating band which indicates that the variation of the antenna does not add any pernicious phase distortion to the incoming/outgoing signals.

To highlight the advantages, the performance of the studied antenna in-terms of size, electrical dimensions, operating band, bandwidth, bandwidth dimension ratio (BDR), and peak gain have been compared with recently reported SWB/UWB antennas and presented in Table II. BDR indicates that how much operating bandwidth in percentage can be achieved by per unit electrical area of an antenna and its value should be high to substantiate the advantages of the proposed design over other existing designs. The footprint and electrical dimension of the proposed antenna are smaller than those reported in [4 - 22] while achieving higher operating bandwidth, and larger BDR which makes it an efficient node antenna to be used in wireless sensor network applications. Though the antenna reported in [23] achieved higher bandwidth and BDR, it possesses almost

4.5 times larger footprint than the

ISSN 2347–3657
Volume 12,Issue 2,May 2024

proposed one and not suitable for wireless sensor node.

v. CONCLUSION

vi. For wireless sensor networks, the most common services used in commercial, industrial, and military settings, an antenna with a low profile that is fed by CPW is suggested. “The anti-”

One L-shaped and one inverted U-shaped coplanar ground plane make up an ipated antenna, which is formed like a modified vertical bow tie. According to the measurements, the antenna has seven resonant modes, and by combining neighboring resonances, it is able to operate in a super-wide band from 3.035 to 17.39 GHz (14.36 GHz). In both the E and H planes, the antenna shows almost omnidirectional radiation patterns and achieved high gain and efficiency. On top of that, it performs well across the board in the time domain. The suggested asymmetric SWB antenna is a great fit for wireless sensor nodes because to its compact size, straightforward construction, and high data transmission rate, all of which are hallmarks of SWB/UWB technology.

REFERENCES

[1] The article "Applications of wireless sensor networks: An up-to-date survey" was written by D. Kandris, C. Nakas, D. Vomvas, and G. Koulouras in 2020. It can be found in the journal Appl Syst Innov., volume 3, issue 14, pages 1–24. "Review on directional antenna for wireless sensor network applications," IET Communications, vol. 14, no. 5, pp. 715 - 722, 2020, by R. George and T. A. J. Mary. Citation: "Design of a novel compact modified-circular printed antenna for high data rate wireless sensor networks" by M. Chinnasamy, E. F. Sundarsingh, and P. Sankaran, published in 2020 in the International Journal of Radio and Microwave Computing and Aided Engineering, volume 30, issue 10, pages 1–10. A tiny ultra-wideband planar monopole antenna with L-shaped ground plane stubs was described by M. T. Tan, J. Q. Li, and Z. Y. Jiang in their 2010 publication. Journal of Radiofrequency Microwave Computer Aided Engineering, volume 29, issue 11, pages 1–7, 2019. IEICE Electron Expr., 2019, pp. 1–4, "Design of a symmetric open slot antenna for UWB applications" (S. Zhang, Y. Zhong, Y. Zhou, Y. Guo, and C. Ji). "Bandwidth enhancement of a CPW-fed monopole antenna with small fractal elements," International Journal of Electron Communications, vol. 69, no. 2, pp. 590 - 595, 2015, authors H. Fallahi and Z. Atlasbaf. In their 2018 publication "Design of compact UWB monopole planar antenna with modified partial ground plane," Sahoo, Mishra, Mohanty, and Mishra discuss the development of such an antenna. The article is found in

ISSN 2347–3657
Volume 12,Issue 2,May 2024

Microw Opt Technol Lett., volume 60, issue 3, pages 578-583.
The article "An octagonal ring-shaped parasitic resonator based compact ultrawideband antenna for microwave imaging applications" was published in 2020 in the journal Sensors and authored by A. Hossain, M. T. Islam, A. F. Almutairi, J. S. Mandeep, K. Mat, and M. Samsuzzaman.
The article "Compact high gain UWB antenna using fractal geometry and UWB-AMC" was published in 2019 in the Microw Opt Technol Lett. journal and was co-authored by R. P. Dwivedi and U. K. Kommuri.
The paper "Bird face microstrip printed monopole antenna design for ultra wide band applications" was published in 2016 in the journal Frequenz and was co-authored by M. J. Hossain, M. R. I. Faruque, M. M. Islam, M. T. Islam, and M. A. Rahman.
[11] "A novel modified U-shaped microstrip antenna for super wide band (SWB) applications" (Analog Integr Circ Sig Process., 2020, pp. 571–578) by M. Elhabchi, M. N. Srifi, and R. Touahni.
The paper "A high performance UWB antenna design for microwave imaging system" was published in 2016 in the Microw Opt Technol Lett. journal and was co-authored by M. Z. Mahmud, M. T. Islam, and M. Samsuzzaman.
The article "Circularly polarized planar monopole antenna for ultrawideband applications" was published in the International Journal of Radio and Wireless Computer-Aided Engineering in 2019. It was written by M. Midya, S. Bhattacharjee, and M. Mitra.
"Multi-slot microstrip antenna for ultra-wide band applications," by N. M. Awad and M. K. Abdelazeez, [14] "Journal of King Saud University of Engineering and Technology," 2018, pp. 38–45.
The paper "A compact umbrella shaped UWB antenna for ground-coupling GPR applications" was published in 2018 in the Microw Opt Technol Lett. journal and was written by S. Kundu and S. K. Jana.
[16] "Design of a novel super wideband circular hexagonal fractal antenna," Prog Electromagn Res., vol. 139, pp. 229 - 245, 2013, by M. A. Dorostkar, M. T. Islam, and R. Azim.
The article "Design of CPW-fed antenna with defected substrate for wideband applications" was published in the Journal of Electrical and Computer Engineering in 2016. The authors are A. Sharma, P. Khanna, K. Shingha, and A. Kumar.
Microstrip line-fed printed planar monopole antenna for ultra-wideband (UWB) applications, by R. Azim, M. T. Islam, and N. Misran [18] Published in 2013 by Arab Journal of Science and Engineering, volume 38, issue 9, pages 2415–2422.
As stated in the 2017 article "Top-cross-loop improving the performance of the UWB planar monopole antennas" published in Microw Opt Technol Lett., the authors D. S. Zhang and R. S. Yahya conducted research in this area.
[20] "An ultrawide band monopole

ISSN 2347–3657
Volume 12,Issue 2,May 2024

antenna using hexagonal-square shaped fractal geometry," published in the Journal of Electromagn Waves and Applications in 2020 and with the DOI 10.1080/09205071.2020.1829094, was written by R. Kumar, R. Sinha, A. Choubey, and S. K. Mahto. [21] "UWB coplanar waveguide-fed coplanar strips rectangular spiral antenna," International Journal of Radio and Wireless Computer-Aided Engineering, volume 27, issue 7, pages 1–6, 2017.
The article "Ultra-wideband slotted semi-circular patch antenna" was published in 2014 in Microw Opt Technol Lett. and was written by T. M. Telsang and A. B. Kakade. "A semicircular shaped super wideband patch antenna with high bandwidth dimension ratio" (M. Samsuzzaman and M. T. Islam, 2015, Microw Opt Technol Lett., 57(2), 445–452). [24] "Design optimization of CPW-fed microstrip patch antenna using constrained ABFO algorithm," published in 2018 in Soft Comput., by N. Gupta, J. Saxena, and K. S. Bhatia. IEEE Antennas Wirel Propag Lett., vol. 16, pp. 912 - 915, 2017, A. Lalbakhsh, M. U. Afzal, and K. P. Esselle, "Multiobjective particle swarm optimization to design a time-delay equalizer metasurface for an electroma

[2] gnetic band-gap resonator antenna" [25].